UWB Signal Propagation at the Human Head

Thomas Zasowski, *Student Member, IEEE*, Gabriel Meyer, *Member, IEEE*, Frank Althaus, and Armin Wittneben, *Member, IEEE*

***Abstract*—Among different wireless solutions, ultra-wideband (UWB) communication is one promising transmission technology for wireless body area networks (WBANs). To optimize receiver structures and antennas for UWB WBANs with respect to energy efficiency and complexity, the distinct features of the body area network channel have to be considered. Thus, it is necessary to know the propagation mechanisms in the proximity of the human body. In this paper, we limit ourselves to transmission at the head, since the most important human communication organs, such as the mouth, eyes, and ears, are located there. We especially focus on the link between both ears and consider direct transmission, surface waves, reflections, and diffraction as possible propagation mechanisms. We show theoretically and by measurements, which were performed in the frequency range between 1.5–8 GHz, that direct transmission through the head is negligible due to the strong attenuation. We conclude by process of elimination that diffraction is the main propagation mechanism around the human body and verify these conclusions using a finite-difference time-domain simulation. Based on a second measurement campaign, we derive an approximation of the average power delay profile for the ear-to-ear link and calculate values for mean excess delay and delay spread. Finally, we briefly discuss the impact of the distinct ear-to-ear channel characteristic on the design of a WBAN communication system.**

***Index Terms*—Body area network (BAN), propagation mechanisms, ultra-wideband (UWB).**

I. Introduction

A NUMBER of very promising applications such as health monitoring or ubiquitous computing [1]–[5] wireless body area networks (WBANs) has attracted interest in recent years. In a WBAN, several small nodes are placed directly on the human body or close to it, such as in everyday clothing. Since WBAN nodes get their power from rechargeable batteries or by energy harvesting, it is essential that they are extremely energy-efficient [6]. Besides the energy efficiency, the nodes shall be of low complexity to minimize costs.

Ultra-wideband (UWB) communication is one transmission technology promising low-power consumption [7], interference robustness [8], high local capacity [9], and less complex hardware for WBANs [10]. In particular, impulse-radio (IR) [11] transmission seems to be well suited to reduce complexity, since major parts of narrowband communication systems such as mixers, RF oscillators, or phase-locked loops (PLLs) can be omitted in IR systems [12]. To fulfill the requirements mentioned above on energy efficiency and complexity reduction, the distinct behavior of the propagation channel has to be taken into account. For WBANs, this means that the propagation effects on or around the body have to be known. To obtain insight into the UWB WBAN channel, we perform channel measurements in the frequency range 1.5–8 GHz. Due to the proximity of the most important human communication organs, such as the mouth, eyes, and ears, the head is very attractive for the placement of the transmitter and receiver. Hence, in the following, we focus on propagation effects for antennas mounted on opposite sides of the head. In a first measurement campaign, channel measurements were done in an anechoic chamber with several test persons and, for reproducibility reasons, with a standard anthropomorphic model (SAM) head phantom as well. We show by the process of elimination that diffraction is the dominant propagation mechanism for transmission between both ears. The experimental results are verified theoretically and by means of finite-difference time-domain (FDTD) simulation with a SAM head phantom. We performed a second measurement campaign in the anechoic chamber to determine the average power delay profile (APDP) as well as the mean excess delay and the delay spread for the ear-to-ear link.

Due to rising interest in WBANs, a number of investigations on the UWB BAN channel have been published recently. The impact of the body on UWB transmission was investigated in [13]. However, in that work, only one antenna was fixed directly onto the body, and transmission between two body-mounted antennas was not considered. In [14], channel measurements were performed from 3 to 6 GHz on the front side of the body and around the torso. Main channel parameters such as path loss, delay spread, and mean excess delay were extracted for different distances between both antennas. Another investigation of the UWB BAN channel from 3 to 6 GHz was presented in [15]. There, measurements were performed in an indoor environment to achieve realistic propagation conditions. It was shown that frequency correlation properties of the channel change substantially, and significant variations of signal energy spread in time-delay domain were observed. The impact of different antennas on the BAN channel measurements was presented in [16]. In [17], WBAN channel parameters were derived by means of FDTD simulations in the frequency range from 2 to 6 GHz, showing that no direct transmission through the head takes place. A pathloss model similar to the one in [14] was presented in [18], where the authors additionally investigated movements of the arms in more detail.

The remainder of this paper is organized as follows. In Section II, the measurement setup is described. The attenuation for the ear-to-ear channel is presented in Section III without considering different propagation mechanisms. Keeping this expected

Manuscript received August 10, 2005; revised January 13, 2006. This paper was presented in part at the International Conference on Ultra Wideband, Zurich, Switzerland, September 2005.

The authors are with the Communication Technology Laboratory, Swiss Federal Institute of Technology (ETH Zurich), 8092 Zurich, Switzerland (e-mail: zasowski@nari.ee.ethz.ch).

Digital Object Identifier 10.1109/TMTT.2006.871989

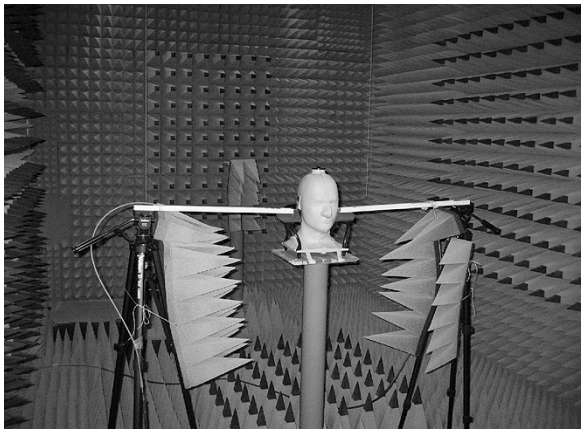

Fig. 1. Measurement setup with SAM head phantom in the anechoic chamber.

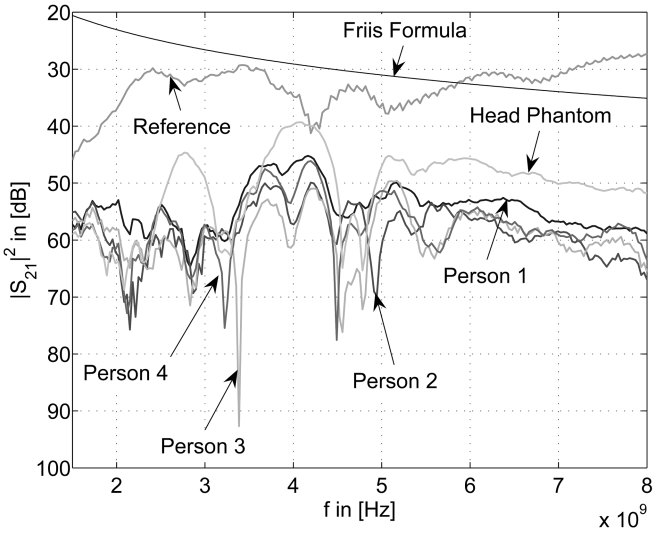

Fig. 2. Frequency transfer functions for different persons and head phantom measured in an anechoic chamber.

attenuation on the human head in mind, in Section IV, dominant propagation mechanisms are determined by a process of elimination based on measurements and calculations. A verification of these results is given in Section V by means of FDTD simulations. In Section VI, mean excess delay and delay spread are calculated, and an approximation of the APDP is derived for the ear-to-ear link. The impact of these results on UWB WBAN communication systems is discussed briefly in Section VII. Conclusions are drawn in Section VIII.

II. Measurement Setup

For determination of the propagation effects, channel measurements were performed with a vector network analyzer (VNA) in the frequency range from 1.5 to 8 GHz using Skycross SMT-3TO10M-A antennas. Such antennas are specified for the frequency range between 3–10 GHz, but it turned out that they can be used also for lower frequencies, where the antennas have a certain attenuation. To reduce the influence of unwanted cable effects on the measurements, the antennas were mounted on glass-fiber reinforced plastic (GRP) arms on tripods, as shown in Fig. 1. The tripods were covered by absorbing material to reduce reflections caused by them. With such a measurement setup, only the antennas were placed close to the head, while the cables led away from the head as quickly as possible.

Measurements were performed with four different test persons and, for reproducibility reasons, also with a SAM head phantom V4.5 from SPEAG [19]. The phantom was filled with the head tissue simulation liquid HSL 5800, which consists of water, mineral oil, emulsifiers, additives, and salt. This lossy dielectric liquid matches the requirements according to the FCC [20] in the frequency range from 4.9 to 6.0 GHz. At 5.2 GHz, relative permittivity is given by $\varepsilon_r = 36.0$ and conductivity by $\sigma = 4.66$ S/m and, at 5.8 GHz, by $\varepsilon_r = 35.3$ and $\sigma = 5.27$ S/m, respectively. As shown in Fig. 1, the head phantom was placed on a plastic pillar for the measurements.

III. Atenuation at the Head

In Fig. 2, frequency transfer functions are shown for the four different persons and the head phantom. It can be seen that the transfer functions for all test persons are similar. The transfer function for the head phantom shows also a similar shape. However, for a wide range of frequencies, the attenuation is about 5–10 dB smaller compared with that for the test persons. Although the liquid inside the head phantom is only specified for the frequency range 4.9–6 GHz, it seems to fit the attenuation characteristic of a human head over a wider frequency range. For comparison reasons, the attenuation calculated with Friis' formula for an isotropic antenna and a reference measurement without head are shown in Fig. 2. The difference between attenuation of the reference measurement and the one calculated with Friis' formula is mainly caused by the gain variations of the antennas. At the lower end of the considered frequency band, we are in the Fresnel zone of the antenna. Above 3 GHz, the gain of the antenna is increasing due to a constant size of the antenna but decreasing wavelength. For the head measurements, an attenuation of about 20–30 dB higher compared with the reference measurement and attenuation derived from Friis' formula can be observed.

IV. Propagation Mechanisms

A. Direct Transmission Through the Head

We start the propagation mechanism investigations by considering direct transmission through the head first. Wavelength and propagation speed of electromagnetic waves depend on the material parameters of the propagation medium. Thus, the expected difference in the arrival time of a direct path through the head and the reference path through the air can be calculated according to (1). Based on the permittivity and conductivity values given for the head phantom, a direct path through the head would have an expected delay of

$$\Delta t = \frac{d}{v_{\text{head}}} - \frac{d}{c} = 2.92\ \text{ns} \tag{1}$$

compared to the direct path of a reference measurement without head. In (1), $v_{\text{head}} = 4.88 \cdot 10^7$ m/s denotes the propagation speed through the head, $c = 3 \cdot 10^8$ m/s denotes the speed

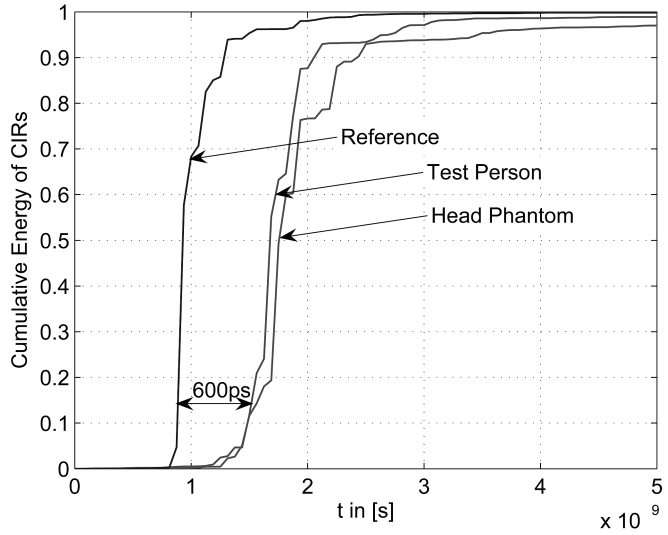

Fig. 3. Cumulative energy of CIRs for transmission with and without head.

of light, and $d = 0.17$ m denotes the distance between both antennas.

In Fig. 3, cumulative energies of channel impulse responses (CIRs) measured in an anechoic chamber with and without head are plotted. We assume that the first paths of the CIRs are at the time instances where the first significant increase of energy can be observed. It can be seen that the cumulative energy distributions are relatively similar for the test persons and head phantom. However, the first paths of those CIRs are delayed by only about 600 ps compared with the reference measurement. This delay of the first paths is much smaller than the calculated delay $\Delta_t = 2.92$ ns in (1). Since the cumulative energy plots for the head in Fig. 3 show no significant increase of energy at the expected delay from (1), we conclude that transmission through the head is negligible.

To verify the result that transmission through the head is negligible, we calculate the attenuation for transmission through the head. For this purpose, we consider the head as a lossy medium. Such a lossy medium can be described by its complex permittivity

$$\begin{aligned}\underline{\varepsilon}_r &= \varepsilon_r' - j\varepsilon_r'' \\ &= \varepsilon_r\left(1 - j\frac{\sigma}{\omega\varepsilon_0\varepsilon_r}\right) \\ &= \varepsilon_r(1 - jd_\varepsilon)\end{aligned} \tag{2}$$

where ε_r' and ε_r'' determine the dispersion and losses respectively, and its complex permeability

$$\underline{\mu}_r = \mu_r' - j\mu_r'' = \mu_r(1 - jd_\mu) \tag{3}$$

where ε_r' and μ_r' correspond to the relative permittivity ε_r and the relative permeability μ_r of the lossless medium, respectively [21]. Using (2) and (3), the wavenumber

$$\underline{k} = k' - jk'' = \omega\sqrt{\varepsilon_0\underline{\varepsilon}_r\mu_0\underline{\mu}_r} \tag{4}$$

becomes complex. ε_0 and μ_0 denote permittivity and permeability in free space, respectively. Thus, the electrical field strength of a wave in a lossy medium can be described as a function of the propagation distance z by

$$E(z,t) = \underline{E}\cdot e^{(j(\omega t - \underline{k}z))} = \underline{E}\cdot e^{-k''z}\cdot e^{\left(j(\omega t - k'z)\right)} \tag{5}$$

where $\underline{E}$ is the electric field-strength, the angular frequency is given by $\omega = 2\pi f$, and time is given by t. In (5), $e^{-k''z}$ depicts the attenuation term containing

$$k'' = \frac{2\pi}{\lambda_\varepsilon}\cdot\Im\left\{\sqrt{1 - jd_\varepsilon}\right\} \tag{6}$$

where $\Im\{\cdot\}$ denotes the imaginary part of the argument. The wavelength λ_ε in a lossy dielectric is given by

$$\lambda_\varepsilon = \frac{\lambda_0}{\sqrt{\varepsilon_r}\cdot\Re\left\{\sqrt{1 - jd_\varepsilon}\right\}} \tag{7}$$

where $\Re\{\cdot\}$ is the real part of the argument. From (2), we get

$$d_\varepsilon = \frac{\sigma}{\omega\varepsilon_0\varepsilon_r} \tag{8}$$

where $\lambda_0 = 0.06$ m, which corresponds to a frequency $f_0 \approx 5.2$ GHz, $\varepsilon_0 \approx (10^{-9}/36\pi)$(As/Vm), $\mu_0 = 4\pi 10^{-7}$(Vs/Am), and $\mu_r \approx 1$, and, using the relative permittivity and conductivity for the head phantom specified, we get from (6)

$$k'' \approx -146.4\frac{1}{\mathrm{m}}. \tag{9}$$

Putting this result in the attenuation term $e^{-k''z}$ in (5), the attenuation for a distance of $z = 0.17$ m, which corresponds to the distance between the antennas on the head, becomes

$$e^{k''z} = e^{146.4\frac{1}{\mathrm{m}}\cdot 0.17\ \mathrm{m}} \approx 216.2\ \mathrm{dB}. \tag{10}$$

Since relative permittivity and conductivity of the head phantom are very similar to human head tissues (cf. [22]), this result can be regarded also as valid for transmission through human heads. The calculations above show that the direct component of a transmission through the head is attenuated severely. This attenuation is much higher than expected from the transfer function plots in Fig. 2. Thus, we again conclude that energy transmitted through the head is negligible and that there have to exist other propagation mechanisms around the head, which cause the only slightly delayed transmission paths in Fig. 3.

B. Surface Waves

Since the human head consists of several layers of different tissues, surface waves are one possible propagation mechanism around the head. Surface waves travel along the boundary between two different media [21] and along curvatures. It is possible to measure surface waves by channel measurements

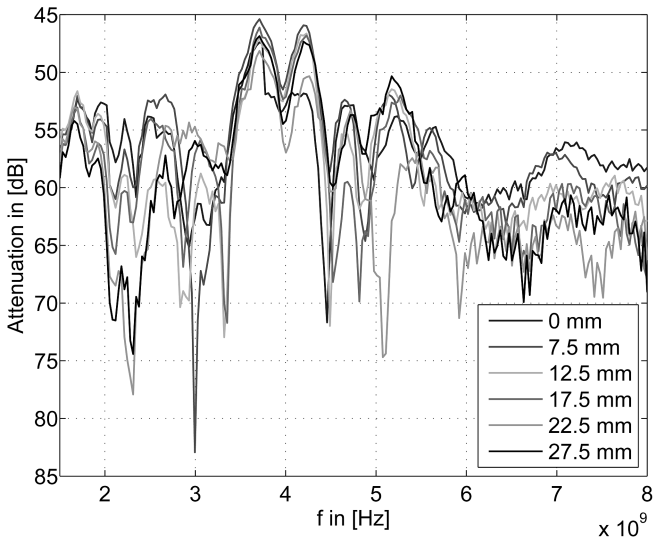

Fig. 4. Transfer functions for different distances between antennas and head surface.

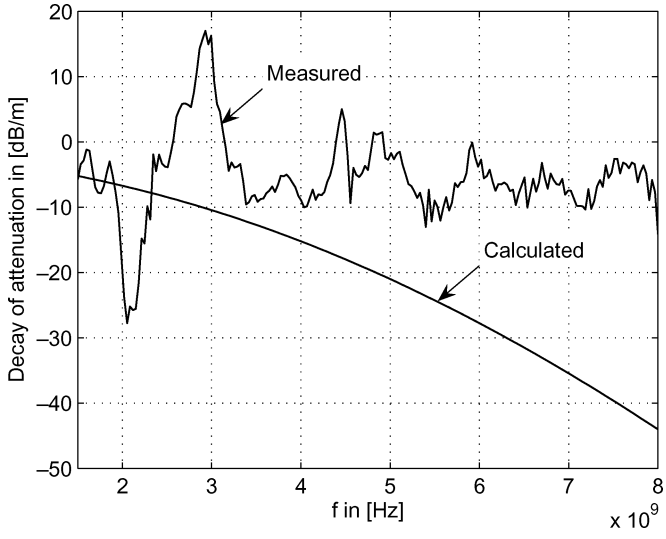

Fig. 5. Calculated and measured decays of attenuation.

with different distances between antennas and surface. If surface waves exist, then the electromagnetic field decays exponentially when the field detector is moving away from the boundary between two tissues [23]. Hence, we performed further channel measurements moving the antennas away from the head. For several distances between the head and antennas, the transfer functions were measured. In Fig. 4, exemplary transfer functions on the head are shown for changing distances between both antennas and the skin. Since the transfer functions are plotted in a logarithmic scale, the attenuation should increase linearly with increasing distance if there exist surface waves around the head. The exponential decay of the field strength caused by surface waves is frequency-dependent and can be calculated from the field component (cf. [23])

$$E_x \sim e^{-\Re\{u\}y}. \tag{11}$$

Equation (11) can be solved by inserting the distance y between antenna and surface and

$$u = \sqrt{\frac{k_1^2 - k_2^2}{1 - \left(\frac{k_1^2}{k_2^2}\right)^2}} \tag{12}$$

with the squared wavenumber $k_1^2 = -j\omega\mu_0(\sigma + j\omega\varepsilon_0\varepsilon_r)$ for the tissue and the squared wavenumber $k_2^2 = \omega^2\mu_0\varepsilon_0$ for air.

From (11), it can be seen that the field strength attenuation is increasing exponentially, i.e., linearly in logarithmic scale, with increasing distance for a fixed frequency. Since the wavenumbers in (12) are frequency-dependent, the slopes of the field strength attenuation not only depend on the distance but also on the frequency. It follows from (12) that the slopes of the field strength attenuation over the distance become steeper with increasing frequency. This can be observed from Fig. 5, in which the slopes of the field strength attenuation are shown as calculated from (11) with frequency-dependent tissue values given in [22]. For the measurements, the slopes of the field strength attenuation over the distance are fitted for each frequency by using a least-square method. These slopes of attenuation approximated from the measurements are also plotted in Fig. 5 and do not exhibit an increase of the slope over distance with increasing frequency. For some frequencies, even a decrease of attenuation with distance can be observed. Only for frequencies between approximately 1.5 and 1.9 GHz, calculated and measured decays of attenuation are in the same order of magnitude, i.e., no relevant surface waves can be detected in the frequency range between 1.9–8 GHz.

Moreover, surface waves are traveling with a speed slower than light [23] which does not explain the slightly delayed first paths for the head measurement in Fig. 3. Thus, we conclude that surface waves are not the dominant propagation mechanism around the human body and that there have to exist some other dominant propagation mechanisms.

C. Reflection and Absorption

To verify if there exist any reflections or absorptions by the head, we measured the antenna pattern for the antenna mounted on the head phantom and compare it with the antenna pattern without head phantom. The antenna patterns were measured in the anechoic chamber with a VNA. The head with antenna and the antenna alone were mounted on a rotating table, respectively. The measurement setup is shown schematically in Fig. 6 from a top view. Please note that the antennas are not placed in the rotating axis since the center of the head is placed at this point. The excentricity of the reference curves in Figs. 7 and 8 is caused by this head mount. Antenna patterns measured with and without the head are shown exemplarily for frequencies 4.1 and 6.05 GHz, which lie in the currently ECC-envisioned UWB bands in Europe [24], shown in Fig. 7. For the antenna pattern measurement with head phantom, the antenna was mounted on the left ear, as shown in Fig. 6, i.e., for $\varphi \approx 90°$, the head is located between both antennas, while there exists a line-of-sight (LOS) link for $\varphi \approx 270°$. It can be observed that the attenuation measured with head-mounted antenna is less than that for

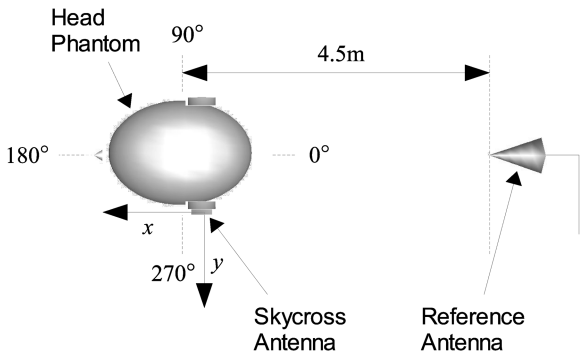

Fig. 6. Schematic measurement setup for antenna pattern measurements with a head phantom (top view).

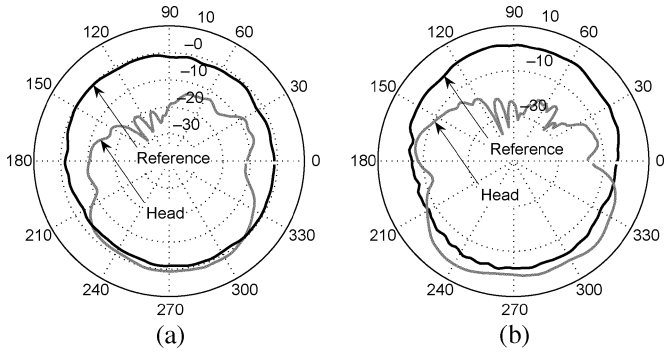

Fig. 7. Antenna pattern with an antenna placed directly on the head and the reference antenna pattern without the head at: (a) $f = 4.1$ GHz and (b) $f = 6.05$ GHz.

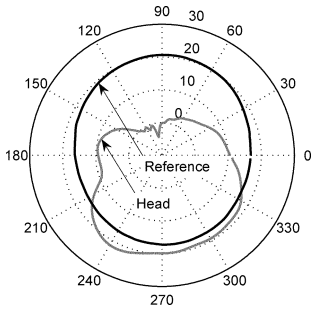

Fig. 8. Energy pattern with an antenna directly placed on the head and a reference energy pattern without the head.

the reference measurement if an LOS link exists. This points to a reflection-like effect caused by the head. If the head acts as an obstacle between the reference antenna and the antenna mounted on the head, i.e., no LOS link exists, then the attenuation measured with the head-mounted antenna is much higher compared to the reference measurement. Similar to the observations in [13], attenuations of up to 20–30 dB can be observed for such a case. Since the antenna patterns in Fig. 7 are only exemplary snapshots, we also consider the energy pattern to take the wideband characteristics of UWB into account. The energy pattern descriptor [25] integrates the power density radiated by the

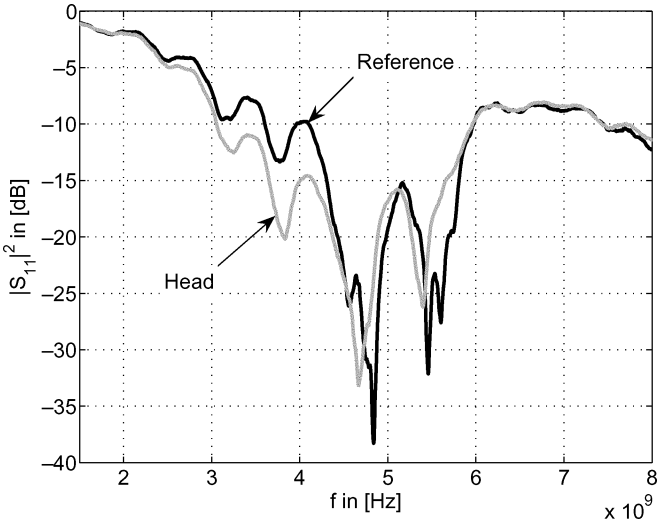

Fig. 9. S_{11}-parameter for an antenna placed directly on the head and for an antenna without the head as reference.

antennas over the whole time or frequency, respectively. Hence, the energy pattern is defined as

$$U(\theta) = \int_{-\infty}^{\infty} |h(t,\theta)|^2 \, dt = \int_{-\infty}^{\infty} |H(f,\theta)|^2 \, df \qquad (13)$$

where $h(t)$ denotes the measured channel impulse response and $H(f)$ denotes the corresponding frequency transfer function. In the following, we use the frequency band between 1.5–8 GHz as the integration limits. Since often noncoherent receivers such as an energy detector or a transmitted-reference receiver [26] are envisioned for use in UWB BANs, such an energy pattern is of particular interest because it shows the whole energy that can be collected from one direction. The normalized energy pattern in Fig. 8 shows a characteristic similar to the antenna patterns in Fig. 7. For angles between approximately 210° and 330°, the energy pattern of the head measurement exceeds the energy pattern of the reference measurement, and reflection effects can be supposed. For the remaining angles, the attenuation measured with a head-mounted antenna is much higher than that for the reference measurement. This means that not much energy is collected if the head is located between the reference and head-mounted antenna.

In Fig. 9, the forward reflection coefficient S_{11} is shown for an antenna directly mounted on the head. For comparison, the coefficient S_{11} is also depicted for a reference measurement without the head. Only slight differences between the reference and head measurement can be observed for frequencies below 3 GHz and above 6 GHz. Between 3–6 GHz, the shapes of both curves are also similar, although variations of up to 10 dB can be observed. Between 2.5–4.6 GHz, the antenna match is even better if the antenna is mounted on the head compared with the reference, i.e., more power is radiated by the antenna. From the observation in Fig. 7 that reflections from the head are present for LOS links and from the results in Fig. 9, we conclude that reflection and absorption effects exist on the human head. However, for the envisioned propagation scenario, from one side of the head to the opposite, reflection and absorption play only a subsidiary role.

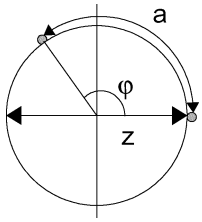

Fig. 10. Schematic assumed for calculation of diffraction around a circular cylinder according to (15).

D. Diffraction

It was shown in the previous sections that neither direct transmission nor surface waves are the dominant propagation mechanism on the human head. Although reflections of the human head can be observed, this propagation mechanism can be neglected for transmission from one side of the head to the opposite. Thus, diffraction remains a possible candidate. If the direct path between the transmitter and receiver is obstructed by an obstacle, waves can travel into the shadow zone behind the obstacle. This kind of diffraction is then also called "creeping" waves [27]. However, diffraction effects are only relevant if the obstacle dimensions are not greater than approximately 60 times the wavelength [28]. This is fulfilled in our case where the wavelengths remain above about $\lambda = 3$ cm. Since diffracted waves travel with the speed of light, the additional path length compared with the reference path length can be calculated from the time delays in Fig. 3. There, it can be observed that the first paths for transmission on the head are delayed by about 600 ps compared with the reference path. Such a delay corresponds to a way that is about

$$\Delta z = 600 \cdot 10^{-12}\ \mathrm{s} \cdot 3 \cdot 10^{8}\ \mathrm{m/s} = 0.18\ \mathrm{m} \tag{14}$$

longer than the direct path of $z \approx 0.17$ m. The increased path length corresponds with the distance between both ears on the head surface. This indicates that diffraction is probably the dominant propagation mechanism.

If we consider the head as circular cylinder with diameter z for simplicity, equations given in [29] can be used to determine the field in the shadow region caused by one ray and, hence, the attenuation of a diffracted wave around the cylinder. For both antennas placed directly on the cylinder surface, as shown in Fig. 10, the field is approximated depending on the angle φ by

$$H(\varphi) \approx -q \cdot e^{-jka} \int_{-\infty}^{\infty} \frac{w_2(\tau)}{w_2'(\tau)} e^{-j\xi\tau} d\tau \tag{15}$$

where k denotes the wavenumber, a is the distance between both antennas on the cylinder surface, and $w_2(\tau) = \sqrt{\pi}(Bi(\tau) - jAi(\tau))$ is the Fock-type Airy function. ξ is given by

$$\xi = \left(\frac{k \cdot z}{4}\right)^{\frac{1}{3}} \cdot \varphi \tag{16}$$

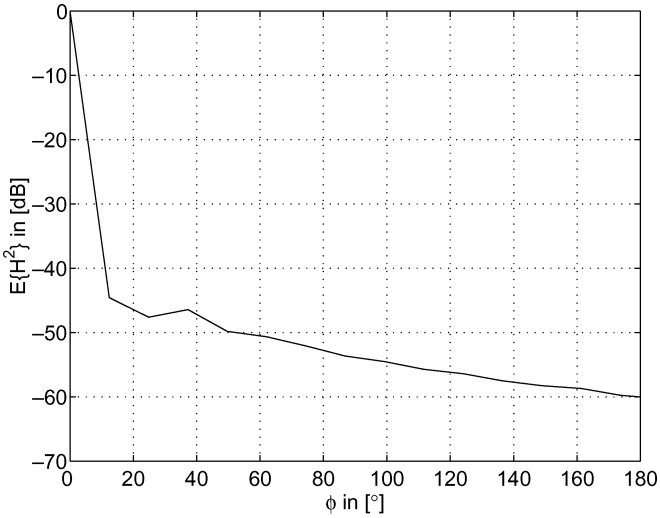

Fig. 11. Attenuation around a cylinder with respect to the angle between both antennas based on (15) and averaged over the frequency range of 1.5–8 GHz.

where φ is the angle between both antennas and q is given by

$$q = \frac{f\varepsilon_0\xi}{\sqrt{2ka}}. \tag{17}$$

Using frequency-dependent values for conductivity and permittivity of brain tissue from [22], the attenuation averaged over the frequency range from 1.5 to 8 GHz is plotted for different angles φ in Fig. 11. As expected, the attenuation is increasing with increasing angle. For $\varphi = 180°$, which corresponds to the case that both antennas are mounted on opposite sides of the cylinder, the attenuation is

$$D = \frac{1}{N_f} \sum_{f=1.5\ \mathrm{GHz}}^{8\ \mathrm{GHz}} \left(|H(\varphi \approx 0)|^2 - |H(\varphi = \pi)|^2\right) \approx 60\ \mathrm{dB}. \tag{18}$$

This calculated attenuation corresponds well with the measured attenuations in Fig. 2.

Of course, for transmission between both ears not only one ray exists, and thus constructive and destructive interference may occur. Nonetheless, we conclude that diffraction is the dominant propagation mechanism around the head due to the following reasons: the path delays correspond well with the increased distances on the head surface, both measurements and calculation show attenuation of same order of magnitude, and other propagation mechanisms can be excluded by process of elimination as described above.

V. Simulation Results

The conclusion from the previous sections is that diffraction is the main propagation mechanism around the head. To verify the measurement results, we also perform FDTD simulations. For this purpose, we are using SEMCAD [30], since a model of the SAM head phantom which we used for the measurements is available in SEMCAD (see Figs. 1 and 12). As for the measurements, the frequency range for the simulation is chosen as 1.5–8 GHz.

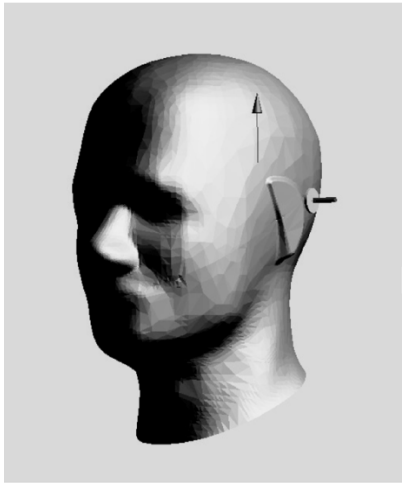

Fig. 12. SAM head phantom used for simulations.

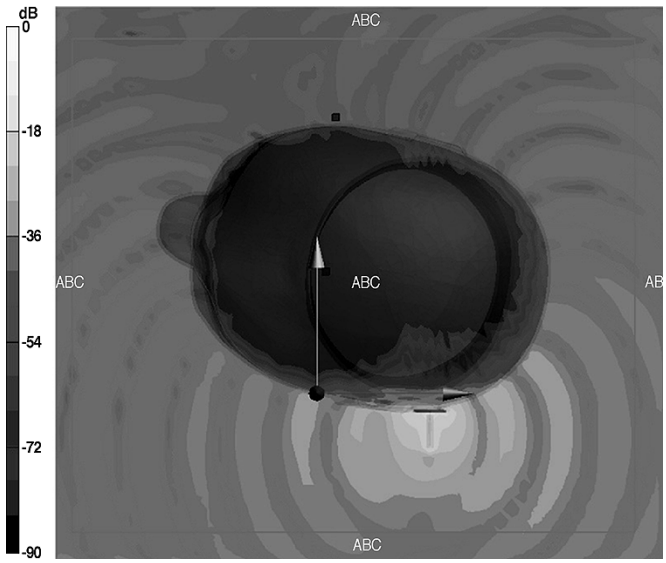

Fig. 13 Simulated field strength in the time domain for the SAM head phantom in the frequency range of 1.5–8 GHz from a top view.

In Fig. 13, a photograph of the simulated field strength in the time domain is shown from the top view. The head is also plotted to show the boundaries of the field inside and outside the head. A monopole, which is placed behind the left ear of the SAM head phantom, is used as a transmit antenna for the simulation. Position and transmit characteristics of the antenna are chosen such that the results are comparable with the measurements.

From the simulation, it can be observed that the field is diffracted around the head, thus supporting the conclusions from the previous sections. The strongest attenuation outside the head can be seen at the right cheek of the head, which is the position on the head with the largest distance from the transmitter on the head surface. For the position behind the right ear, where the receive antenna was placed, an attenuation of about 55–65 dB can be observed. This simulated attenuation corresponds well with the measured attenuation in Fig. 2 and the calculated attenuation from (18). Although a portion of the transmitted power radiates into the head close to the transmit antenna, it can be observed that waves radiated into the head are severely attenuated. Thus, it is verified that direct transmission through the head is negligible, as shown in Section IV-A. From the simulation results, we again conclude that direct transmission through the head is negligible and that diffraction is the main propagation mechanism for transmission between both ears.

VI. Channel Characterization

A second measurement campaign was performed to investigate the ear-to-ear channel characteristic. The measurements were conducted again in the anechoic chamber with the network analyzer in the frequency range between 2 and 8 GHz. The channel between both ears was measured five times each on 11 different persons, resulting in an overall number of 55 measured channel transfer functions.

We use the mean excess delay τ_m, which is the first central moment of $|h(\tau)|^2$ and the delay spread τ_{rms}, which is the square root of the second central moment of $|h(\tau)|^2$, to characterize the power delay profile [31]. The mean excess delay τ_m is defined as

$$\tau_m = \frac{\int_0^\infty \tau \cdot |h(\tau)|^2 \, d\tau}{\int_0^\infty |h(\tau)|^2 \, d\tau} \tag{19}$$

and the delay spread τ_{rms} as

$$\tau_{\mathrm{rms}} = \sqrt{\frac{\int_0^\infty (\tau - \tau_m)^2 \cdot |h(\tau)|^2 \, d\tau}{\int_0^\infty |h(\tau)|^2 \, d\tau}} \tag{20}$$

where $h(\tau)$ is the channel impulse response and τ is the time. For evaluation of τ_m and τ_{rms}, we limit the dynamic range to 50 dB. Averaged over all ear-to-ear measurements, we obtain a mean excess delay $\tau_m = 2.1$ ns and delay spread $\tau_{\mathrm{rms}} = 1.5$ ns. Both values are slightly higher compared with the mean excess delay and delay spread values for a 30-cm LOS link presented in [14]. This is reasonable, since the waves diffract around the head and since the distance between both antennas on the head surface is also slightly higher than 30 cm.

The APDP, averaged over all ear-to-ear measurements, is shown in Fig. 14. The power-delay profiles are aligned at the samples with the highest energy. The APDP does not show a linear decay in the logarithmic domain over the considered dynamic range. There exist two ranges with different linear decays. Up to about 4 ns, the APDP is decaying relatively steep. This is where only transmission around the head takes places. For delays above about 4 ns, the linear decay gets flatter. This flattening is caused by effects such as reflections from the body or also from the environment. Although the measurements were done in an anechoic chamber, in particular, the absorbing material placed on the tripods is only attenuating the waves by about 15 dB and thus can cause reflections.

Due to this behavior of the APDP in the logarithmic scale, the APDP shown in Fig. 14 is approximated by two exponentials for

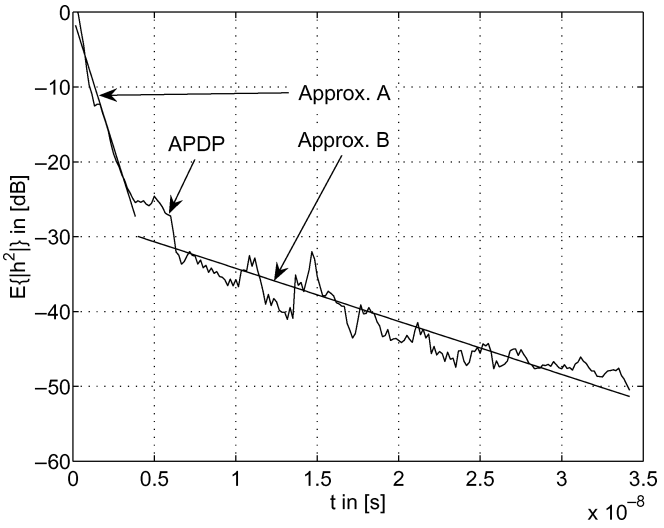

Fig. 14. APDP over all ear-to-ear measurements and approximation of the APDP from (21) and (22).

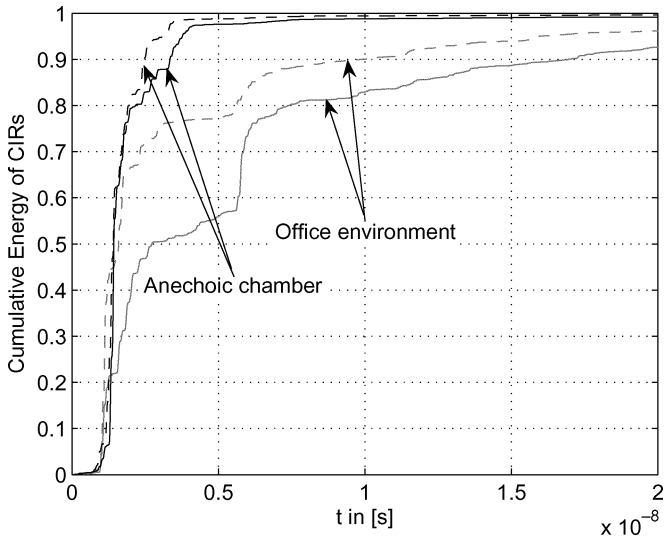

Fig. 15. Cumulative energy of a CIR in an office environment and an anechoic chamber; the antenna's main directivity was changed from horizontal backward (dashed lines) to vertical to the floor (solid lines).

the different ranges. The approximation for the range up to 4 ns is given by

$$A = a_1 - a_2 \cdot t \tag{21}$$

and for the range above 4 ns by

$$B = b_1 - b_2 \cdot t \tag{22}$$

where t denotes the time in seconds. The parameters a_1, a_2, b_1, and b_2 are determined as $a_1 = -0.6$, $a_2 = 7.0 \cdot 10^{-9}$, $b_1 = -27.1$, and $b_2 = 0.7 \cdot 10^{-9}$ using a least-square curve fitting in the logarithmic domain.

From the APDP and the delay spread, it can be concluded that the main energy is contained in a extremely short time interval. Only about 4 ns after the maximum peak the energy is decayed by about 25 dB. This concentration of the energy in a short time window directly influences the design of a communication system, as we show in Section VII.

VII. Impact of Propagation Mechanisms on a BAN Communication System

As shown in [32] and [33], performance of a transmitted-reference (TR) receiver and energy detector (ED) strongly depend on the integration time used in such receivers. It was shown in Section VI that the energy is concentrated in a relatively short time window for the ear-to-ear link. To see the impact of an environment that is different from the anechoic chamber, cumulative energies of CIRs measured in an anechoic chamber and an office environment are plotted in Fig. 15. Dashed lines depict measurements where both antennas' main directivities pointed toward the floor. For the measurements depicted by solid lines, the antennas were rotated such that their main directivities pointed horizontally backward. It can be observed, for the anechoic chamber CIRs, that almost the whole energy is contained in a window of about only 3.5 ns, i.e., the integration length is very small for an ED or TR receiver. Compared with the channel measured in the anechoic chamber, energy can also be captured from multipath reflections in the office environment. In Fig. 15, a path at about 6 ns is particularly obvious. This path is caused by a table in front of which the test person was sitting. For the backward orientation of the antennas, this path is not as strong due to the aforementioned directivity of the antennas. Nevertheless, first paths around the head caused by diffraction can also be observed in the office environment. Using the 3.5-ns window size determined from the anechoic chamber measurements, it is possible to collect approximately 50% and 75% of the whole energy in the office environment, respectively, as shown in Fig. 15. This means that the receiver is made insensitive to environment changes by choosing a very short integration time, i.e., by only collecting energy of paths diffracting around the head.

Of course, an adaptive receiver, which adapts its integration length according to the environment, could achieve better performance. However, due to complexity issues, an ED or TR receiver with a fixed integration length is favorable for use in BANs.

It was shown that direct transmission through the head is negligible and that diffraction is the main propagation mechanism around the head. This has also a strong impact on the design of antennas used in wireless BANs. Antennas should be designed such that almost the whole energy is radiated along the head surface to take advantage of diffraction and neither into the head nor away from the head. With such an antenna, the energy that can be collected from reflections will be reduced. However, this will not influence performance of an ED or TR receiver with a fixed short integration length that only collects energy from paths around the head, as described above. Using antennas that do not radiate away from the head does not only reduce the energy that can be collected from reflections but also reduces interference caused by other wireless systems in close vicinity that

might prohibit UWB communication [8]. Since the surface of the human body looks like a plane for small areas only and usually exhibits curvatures, dipoles or monopoles mounted perpendicular to the body surface are also suited for use in BANs. For such arrangements, energy is radiated along possible curvatures on the body but not directly into the body due to the antenna characteristic.

If energy shall be collected from reflections using an ED or TR receiver with adaptive integration length, antennas isotropically radiating into a half-space away from the head can be used.

VIII. Conclusion

In this paper, we identified the dominant propagation mechanism for the ear-to-ear link at the human head. It was shown that direct transmission can be neglected for transmission from one side of the head to the opposite due to reflections and the strong attenuation of the head. Furthermore, neither surface waves nor reflections and absorptions are dominant for the ear-to-ear link, and we conclude that diffraction is the dominant propagation mechanism around the head. Based on a second measurement campaign, we calculated mean excess delay and delay spread and presented the APDP for the ear-to-ear link. From these investigations, we observed that the most energy in the CIR is contained in a relatively short time window. The performance of noncoherent receivers with a fixed short integration time are not influenced by the environment and therefore are well suited for use in WBANs. Since most energy transmitted into the head is either reflected or absorbed, we concluded that antennas should be designed such that they take advantage of creeping waves, i.e., they do not transmit into the head and therefore help to increase the acceptance of such systems.

References

[1] T. Zasowski, G. Meyer, F. Althaus, and A. Wittneben, "Propagation effects in UWB body area networks," in *Proc. ICU*, Sep. 2005, pp. 16–21.

[2] P. Coronel, W. Schott, K. Schwieger, E. Zimmermann, T. Zasowski, H. Maass, I. Oppermann, M. Ran, and P. Chevillat, "Wireless body area and sensor networks," in *Proc. Wireless World Res. Forum Briefings*, Dec. 2004 [Online]. Available: http://www.wireless-world-research.org/

[3] N. B. Bharatula, S. Ossevoort, M. Stäger, and G. Tröster *et al.*, "Toward wearable autonomous microsystems," in *Pervasive Computing: Proc. 2nd Int. Conf.*, Apr. 2004, pp. 225–237.

[4] J. Bernhard, P. Nagel, J. Hupp, W. Strauss, and T. von der Grün, "BAN—Body area network for wearable computing," in *Proc. 9th Wireless World Res. Forum*, Jul. 2003 [Online]. Available: http://www.wireless-world-research.org/

[5] J. Chiang, W. Akram, T. Johnson, X. Gao, and R. Bhatia, "A wireless motion system for video gaming," in *Proc. ICCE*, Jan. 2005, pp. 425–426.

[6] S. Jung, C. Lauterbach, M. Strasser, and W. Weber, "Enabling technologies for disappearing electronics in smart textiles," in *Proc. IEEE ISSCC*, Feb. 2003, vol. 1, pp. 386–387.

[7] L. Stoica, A. Rabbachin, H. O. Repo, T. S. Tiuraniemi, and I. Oppermann, "An ultrawideband system architecture for tag based wireless sensor networks," *IEEE Trans. Veh. Technol.*, vol. 54, no. 5, pp. 1632–1645, Sep. 2005.

[8] T. Zasowski, F. Althaus, and A. Wittneben, "Temporal cognitive UWB medium access in the presence of multiple strong signal interferers," in *Proc. 14th IST Mobile Wireless Commun. Summit*, Jun. 2005.

[9] V. S. Somayazulu, J. R. Foerster, and S. Roy, "Design challenges for very high data rate UWB systems," in *36th Asilomar Signals, Syst. Comput. Conf. Rec.*, Nov. 2002, vol. 1, pp. 717–721.

[10] D. Porcino and W. Hirt, "Ultra-wideband radio technology: Potential and challenges ahead," *IEEE Commun. Mag.*, vol. 41, no. 7, pp. 66–74, Jul. 2003.

[11] M. Z. Win and R. A. Scholtz, "Impulse radio: How it works," *IEEE Commun. Lett.*, vol. 2, no. 2, pp. 36–38, Feb. 1998.

[12] D. Barras, F. Ellinger, and H. Jäckel, "A comparison between ultra-wideband and narrowband transceivers," in *Proc. TRLabs/IEEE Wireless*, Jul. 2002, pp. 211–214.

[13] T. B. Welch, R. L. Musselman, B. A. Emessiene, P. D. Gift, D. K. Choudhury, D. N. Cassadine, and S. M. Yano, "The effects of the human body on UWB signal propagation in an indoor environment," *IEEE J. Sel. Areas Commun.*, vol. 20, no. 9, pp. 1778–1782, Dec. 2002.

[14] T. Zasowski, F. Althaus, M. Stäger, A. Wittneben, and G. Tröster, "UWB for noninvasive wireless body area networks: Channel measurements and results," in *Proc. IEEE UWBST*, Nov. 2003, pp. 285–289.

[15] I. Z. Kovács, G. F. Pedersen, P. C. F. Eggers, and K. Olesen, "Ultra wideband radio propagation in body area network scenarios," in *Proc. IEEE ISSSTA*, Sep. 2004, pp. 102–106.

[16] A. Alomainy, Y. Hao, C. Parini, and P. Hall, "Comparison between two different antennas for UWB on-body propagation measurements," *IEEE Antennas Wireless Propag. Lett.*, vol. 4, pp. 31–34, 2005.

[17] A. Fort, C. Desset, J. Ryckaert, P. D. Doncker, L. V. Biesen, and S. Donnay, "Ultra wideband body area channel model," in *Proc. IEEE ICC*, May 2005, pp. 2840–2844.

[18] A. Fort, C. Desset, J. Ryckaert, P. D. Doncker, L. V. Biesen, and P. Wambacq, "Characterization of the ultra wideband body area propagation channel," in *Proc. ICU*, Sep. 2005, pp. 22–27.

[19] Schmid & Partner Engineering AG, SPEAG. Zurich, Switzerland [Online]. Available: http://www.speag.com

[20] D. L. Means and K. W. Chan, "Evaluating compliance with FCC guidelines for human exposure to radiofrequency electromagentic fields, additional information for evaluating compliance of mobile and portable devices with FCC limits for human exposure to radiofrequency emissions," *FCC Suppl. C (Ed. 01-01) to OET Bull. 65 (Ed. 97-01)*, pp. 1–53, Jun. 2001.

[21] H. Meinke and F. W. Gundlach, *Taschenbuch der Hochfrequenztechnik, Band 1*, 5th ed. Berlin, Germany: Springer-Verlag, 1992.

[22] FCC, "Tissue dielectric properties calculator," Brooks Air Force Base, San Antonio, TX, Tech. Rep. AL/OE-TR-1996-0037 [Online]. Available: http://www.fcc.gov/fcc-bin/dielec.sh, based on results from "Compilation of the dielectric properties of body tissues at RF and microwave frequencies" by Camelia Gabriel.

[23] H. M. Barlow and J. Brown, *Radio Surface Waves*. Oxford, U.K.: Oxford Univ. Press, 1962.

[24] "Draft of the ECC decision on the harmonised conditions for devices using UWB technology in bands below 10.6 GHz," Electron. Commun. Committee, Copenhagen, Denmark, (ECC/DEC/(06)AA), Nov. 2005.

[25] J. S. McLean, H. Foltz, and R. Sutton, "Pattern descriptors for UWB antennas," *IEEE Trans. Antennas Propag.*, vol. 53, no. 1, pp. 553–559, Jan. 2005.

[26] S. Dubouloz, B. Denis, S. de Rivaz, and L. Ouvry, "Performance analysis of LDR UWB noncoherent receivers in multipath environments," in *Proc. ICU*, Sep. 2005, pp. 491–496.

[27] L. B. Felsen and N. Marcuvitz, *Radiation and Scattering of Waves*, ser. Electromagn. Waves. New York: IEEE Press, 1994.

[28] R. Schmitt, *Electromagnetics Explained, A Handbook for wireless/RF, EMC, and High-Speed Electronics*. Amsterdam, The Netherlands: Elsevier Sci., 2002.

[29] R. Paknys, "Uniform asymptotic formulas for the creeping wave field on or off a cylinder," *IEEE Trans. Antennas Propag.*, vol. 41, no. 8, pp. 1099–1104, Aug. 1993.

[30] Simulation platform for electromagnetic compatibility, antenna design, and dosimetry. SEMCAD [Online]. Available: http://www.semcad.com

[31] J. D. Parsons, *The Mobile Radio Propagation Channel*, 2nd ed. New York: Wiley, 2000.

[32] T. Zasowski, F. Althaus, and A. Wittneben, "An energy efficient transmitted-reference scheme for ultra wideband communications," in *Proc. Joint UWBST IWUWBS*, May 2004, pp. 146–150.

[33] M. Weisenhorn and W. Hirt, "Robust noncoherent receiver exploiting UWB channel properties," in *Proc. Joint UWBST IWUWBS*, May 2004, pp. 156–160.

Thomas Zasowski (S'02) received the Dipl.-Ing. degree in electrical engineering from Saarland University, Saarbrücken, Germany, in 2002, and is currently working toward the Ph.D. degree at the Swiss Federal Institute of Technology (ETH Zurich), Zurich, Switzerland.

Since 2002, he has been with the Communication Technology Laboratory, ETH Zurich. His main research interests are in the field of UWB communications with an emphasis on body area networks.

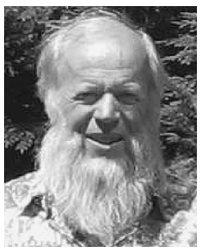

Gabriel Meyer (S'74–M'85) received the Diploma degree in electrical engineering and Ph.D. degree from the Swiss Federal Institute of Technology (ETH Zurich), Zurich, Swizterland, in 1975 and 1985, respectively. His dissertation focused on remote sensing of dielectric bodies.

He joined the Scientific Staff of the Communication Technology Laboratory (CTL), ETH Zurich, where he is engaged with teaching and research in the area of wave propagation and electromagnetic compatibility (EMC). From 1991 to 2003, he was Head of the Wave Propagation and EMC Group, CTL.

Dr. Meyer is an Associate Editor of the IEEE TRANSACTIONS ON ELECTROMAGNETIC COMPATIBILITY. He is a national representative of URSI Commission E. He was chairman of the EMC Zurich Symposium. He was also the organizing chairman of the IEEE International Conference on Ultra-Wideband (ICU 2005).

Frank Althaus received the Dipl.-Ing. and Dr.-Ing. degrees in electrical engineering from Saarland University, Saarbrücken, Germany, in 1998 and 2002, respectively.

Since 2002, he has been a Research Assistant with the Swiss Federal Institute of Technology (ETH Zurich), Zurich, Switzerland. He is leader of the Ultra-Wideband Group, Communication Technology Laboratory, ETH Zurich.

Dr. Althaus served as the technical co-chair of the IEEE International Conference on Ultra-Wideband (ICU 2005).

Armin Wittneben (M'86) received the Dipl.-Ing. and Doctorate degrees in electrical engineering and Venia Legendi degree in communication technology from the Technical University Darmstadt (TUD), Darmstadt, Germany, in 1983, 1989, and 1997, respectively.

He is a Full Professor of wireless communication with Eidgenössische Technische Hochschule (ETH) Zürich, Zürich, Switzerland, and Director of the Institute of Communication Technology. From 1989 to 1998, he was with Ascom Tech, Maegenwil, Switzerland, where he was in charge of wireless communications research activities. During this time, his department demonstrated, among others, the first Hiperlan/I modem and the fastest modem worldwide for digital powerline communication. In 1998, he became a Full Professor of communications with Saarland University, Saarbrücken, Germany. In 2002, he joined ETH Zürich. His research focuses on cooperative wireless communication, communication theory, digital signal processing, multiple-input–multiple output (MIMO) wireless and UWB wireless.